Potential Oscillations during the Electrocatalytic Oxidation of Sulfide on a Microstructured Ti/Ta_2O_5-IrO_2 Electrode

Aicheng Chen* and Brad Miller

Department of Chemistry, Lakehead University, Thunder Bay, Ontario P7B 5E1, Canada

Received: September 3, 2003; In Final Form: November 7, 2003

The electrooxidation of sulfide on a microstructured oxide electrode $Ti/Ta_2O_5-IrO_2$ was studied using electrochemical methods such as cyclic voltammetry, differential capacity, galvanostatic measurements and electrochemical impedance spectroscopy (EIS). Sulfide and hydrosulfide can be oxidized to sulfur, polysulfides, and sulfate depending upon the electrode potential. Our surface analysis illustrates that the $Ti/Ta_2O_5-IrO_2$ electrode prepared in this study has a "cracked mud" structure with oxide particles sitting on the top of the electrode surface which have a particle size of around 100 nm. For the first time, two distinct galvanostatic potential oscillations, named as Oscillation A and Oscillation B, respectively, are observed during the electrooxidation of sulfide on an oxide electrode. The features of the potential oscillations strongly depend on the applied current densities. Oscillation A, located in the low current region, has larger amplitudes and much smaller frequencies than Oscillation B, which occurs in the high current region. Our EIS studies show that both Oscillation A and Oscillation B can be classified into HNDR (hidden negative differential resistance) oscillators with oxygen evolution involved. Oscillation A is caused by the variation of the S^{2-}/HS^- surface concentration from the diffusion-limited depletion by oxidation and from the convection-induced replenishment by periodic oxygen evolution, while Oscillation B is due to the synergic effect of sulfur formation/removal and constant oxygen evolution.

1. Introduction

Electrochemical reactions are attractive in nonlinear dynamic studies as current and electrode potential can be easily monitored.[1−3] Oscillations have been observed in a variety of electrochemical systems, which can be divided into anodic metal dissolution (e.g., Fe, Cu, Ni, Sn, Zn),[4−5] anodic oxidation of small molecules (such as ethylene,[6] formate,[6] formaldehyde,[7−8] formic acid,[9−11] methanol,[12] and hydrogen[13−14]), and cathodic reduction of hydrogen peroxide,[15−17] persulfate,[18] and iodate.[19−21] The electrodes used in the above electrochemical oscillators, except for those of metal dissolution, are mainly poly- or single-crystal platinum electrodes. For instance, Ross et al.[9] investigated the effect of rotation and temperature on oscillatory behavior in the electrochemical oxidation of formic acid on Pt(100). Strasser and co-workers[10,11] studied the effect of surface structure on the oscillatory instabilities during formic acid oxidation using Pt(100), Pt(110), and Pt(111) electrodes.

In this paper, we report potential oscillations during the electrooxidation of sulfide on a microstructured oxide electrode $Ti/Ta_2O_5-IrO_2$, which possesses dramatically different properties from a planar Pt electrode. The adsorption of ions and molecules on Pt electrodes is much stronger than that on the oxide electrode surface. Oxide electrodes are an important category of electrode materials which are widely used in many electrochemical processes including electrowinning, cathodic protection,[22] and remediation technology for a cleaner environment,[23−24] as well as in the chlor−alkali industry.[25]

Significant work has been done in the mechanistic classification of electrochemical oscillators[1,26] and in understanding the origin of electrochemical oscillations.[11,19,27] Initially electrochemical oscillatory systems were classified mechanistically as either chemical or electrochemical in nature.[2] Whereas in the former case the chemical autocatalysis was accompanied by chemical charge-transfer steps at the electrode which caused the instability/oscillation, in the latter case it is a combination of both chemical and electrochemical conditions that drives the system away from stable states. This initial scheme was then expanded upon by Koper[27−29] to include negative differential resistance (NDR) electrochemical oscillations, where three classes of oscillators were categorized: oscillators that oscillate under strictly potentiostatic conditions, oscillators that oscillate under potentiostatic conditions with the presence of an ohmic resistance, and oscillations under both potentiostatic and galvanostatic conditions. Strasser et al. further developed this last class of oscillation by the inclusion of mechanistic features (such as faradic processes) in association with the presence of NDR oscillations. This is called a hidden negative differential resistance (HNDR) type oscillation.[10−11,30−32] Although the conditions for the appearance of an HNDR are the same as those of the NDR class, the behavior of these two oscillators is significantly different.[32] In the case of an NDR, only current oscillations will appear on the negative slope of an I/Φ curve. Alternatively, HNDR current oscillations can occur on the positive slope of an I/Φ curve and have a potentiostatic Hoph bifurcation (HB) associated with them.[32] In addition, an HNDR oscillator may generate galvanostatic potential oscillations. The HNDR class is further divided into three sub classes.[32] It has been shown by Koper et al.[26−27,29] that electrochemical impedance spectroscopy (EIS) is a powerful technique in stability study and categorization of electrochemical oscillators. In this study we use EIS to determine the nature of the potential oscillations during the anodic oxidation of sulfide.

* Corresponding author. E-mail: aicheng.chen@lakeheadu.ca.

10.1021/jp036639h CCC: $27.50
Published on Web 01/22/2004

Sulfide is most often encountered as a waste product of the pulp and paper, petroleum, and mining industries. Organic decomposition is another major source of sulfide. Sulfur compounds in transportation fuels remain a major source of air pollution. The largest concern from a public standpoint is the unpleasant odor and high toxicity of H_2S. Electrochemistry provides a tremendous opportunity for treating sulfide waste streams as sulfide and hydrosulfide can be oxidized to sulfur, polysulfides, and sulfate, depending on the electrode potential and temperature of the electrolyte. It has been reported that polysulfides used in the pulp and paper industry can improve the yield and quality of paper.[33] In addition, the oxide electrode $Ti/Ta_2O_5-IrO_2$ is a promising electrocatalyst for the electrochemical treatment of sulfide. For all these reasons, it is important to investigate the electrochemical oxidation of sulfide on oxide electrodes.

In the present work, cyclic voltammetry, linear galvanic voltammetry, differential capacitance measurements, galvanostatic technique, and electrochemical impedance spectroscopy were used to investigate the electrooxidation of sulfide on the $Ti/IrO_2-Ta_2O_5$ oxide electrode. Scanning electron microscopy (SEM) was employed to determine the morphology and surface structure of the oxide. The objectives of this study are (1) to determine the oscillatory instabilities during sulfide oxidation on the oxide electrode, (2) to decipher the origin of the potential oscillations, and (3) to investigate the mechanisms of the anodic oxidation of sulfide.

2. Experimental Section

A three-electrode cell system was used in this study. The working electrode $Ti/IrO_2-Ta_2O_5$ was prepared by a thermal decomposition technique. The electrochemical experimental methods and the procedure of the oxide coating are described in refs 34 and 35. The Ti substrate was polished first using silicon carbide grit 600 powder and followed by diamond compound grade 1 (particle size $< 2\ \mu$m), then etched in 32% HCl at approximately 85 °C for 15 min. The coating solution was made by mixing iridium precursor solution (dissolving 0.30 g of $IrCl_3 \cdot 3H_2O$ in 2.5 mL of ethanol) and tantalum precursor solution (0.13 g $TaCl_5$ dissolved in 7.5 mL of 2-propanol). The mixture of the precursor solution was painted on the pretreated Ti substrate; the solvent was evaporated at around 80 °C by an air stream and then calcinated at 500 °C for 10 min. This procedure was repeated until the oxide coating load reached around 28.0 g/m^2. A final 1 h post-bake at 530 °C completed the procedure. The microstructure of the etched Ti substrate and the oxide coating were characterized by JEOL 5900LV scanning electron microscopy and X-ray energy dispersive spectrometry (SEM/EDX). The geometric surface area of the working electrode was 1.0 cm^2. The counter electrode was a Pt coil. Before each experiment the counter electrode was cleaned by flame annealing and then quenched with Millipore water. The reference electrode was a saturated calomel electrode (SCE) connected to the investigated solution through a salt bridge.

The electrochemical experiments such as cyclic voltammetry (CV), differential capacity (DC), galvanostatic measurement, and electrochemical impedance spectroscopy (EIS) were performed using a VoltaLab 40 potentiostat PGZ301. Electrochemical software VoltaMaster 4 (Version 5.1) was used for data acquisition. The amplitude of the modulation potential for both DC and EIS measurements was 10 mV; the frequency for the DC experiment was 25 Hz and the range of the frequency used for EIS study was from 25 kHz to 25 mHz. The sulfide solution was made by reagent-grade sodium sulfide crystal $Na_2S \cdot 9H_2O$ (Caledon Laboratories Ltd.) with pure water obtained by the purification of deionized water with Milli-Q water purification (17.6 MΩ cm). The concentration of the sodium sulfide solution used in this study was 0.65 M. For comparison, a 0.65 M NaOH solution was also made from reagent-grade sodium hydroxide (Anachemia). An Orion Research model SA 250 was used to measure the pH of the investigated solutions. All solutions were deaerated with ultrapure argon before measurements, and argon was passed over the top of the solution during the experiment. All measurements were conducted at room temperature (20 ± 2 °C).

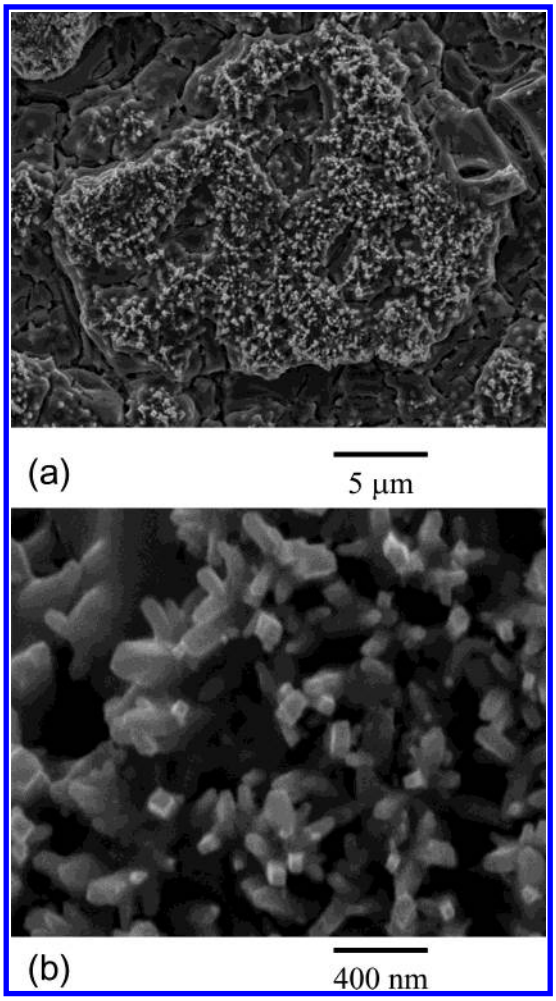

Figure 1. Scanning electron micrographs of Ta and Ir oxide based electrodes ($Ti/Ta_2O_5-IrO_2$). (a) Magnification: ×3000; (b) Magnification: × 35 000.

3. Results

3.1. Microstructure of the Coatings. The surface morphology of the $IrO_2-Ta_2O_5$ oxide coatings was examined by scanning electron microscopy (SEM). As shown in Figure 1a, the oxide coatings exhibit a typical porous "cracked mud" structure. This is consistent with the observation by Comninellis et al.[36] Sitting on the cracked mud are some oxide particles. Figure 1b shows that the size of the particles is between 100 and 150 nm. The above images indicate that the $IrO_2-Ta_2O_5$ oxide electrode prepared in this study has a much larger surface area compared to a planar metal electrode surface such as Pt and Au. A large electrode surface area is desirable for most industrial electrochemical processes. Our further EDX analysis of the oxide coating shows that the content of iridium in the

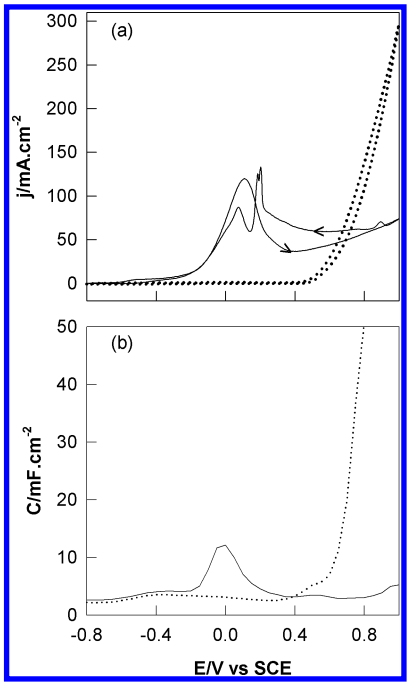

Figure 2. (a) Cyclic voltammograms of 0.65 M Na_2S (solid line) and 0.65 M NaOH (dotted line) at a potential sweep rate of 20 mV/s and (b) differential capacitance plots of 0.65 M Na_2S (solid line) and 0.65 M NaOH (dotted line).

crystal particles is much richer than that in the cracked mud oxides.

3.2. Cyclic Voltammetry and Differential Capacity. Figure 2a shows two cyclic voltammograms (CVs) recorded in 0.65 M Na_2S (solid line) and 0.65 M NaOH (dotted line) solutions. The pH of the sulfide solution is close to that of the 0.65 M hydroxide solution, indicating that HS^- ions are the major sulfide species in the 0.65 M Na_2S solution. As seen by the CV curve in the sodium hydroxide solution, oxygen evolution occurs at around 0.5 V/SCE and, by further increasing electrode potential, the current of the oxygen evolution linearly increases. All these results indicate that the Ti/Ta_2O_5−IrO_2 electrode possesses high electrocatalytic activity for oxygen evolution. In the presence of sulfide (solid line), by sweeping the potential from −0.8 V to 1.0 V/SCE, a broad hump starting at −0.62 V/SCE was observed in the CV, followed by a large and wide peak. This may be due to the oxidation of HS^- ions to polysulfides and sulfur.[37−38] The broad hump may be due to sulfide adsorption and/or polysulfide formation. The large (irreversible) peak may correspond to sulfide oxidation. When scanning back from 1.0 V to −0.8 V/SCE, three peaks at approximately 0.9, 0.2, and 0.05 V are observed in the CV curves. The multiple-peaks shown in the CV curves indicate that a number of different oxidation state sulfur compounds could be formed during the electrooxidation of sulfide. Figure 2b shows two differential capacity (DC) curves determined from the AC impedance measurements using 0.65 M Na_2S (solid line) and 0.65 M NaOH (dotted line) solutions. The shape of these two DC curves is very consistent with the positive-going section of the CV curves shown in Figure 1a, which indicates that both cyclic voltammetry and differential capacity can be used to generally characterize the electrode surface and the electrooxidation of sulfide. Please note, the capacitance of this Ti/Ta_2O_5−IrO_2 electrode is 215 μF cm^{-2} at the electrode potential −0.75 V/SCE as seen in Figure 2b; in contrast, our study shows that the capacitance of Pt is 4.78 μF cm^{-2} at the same potential, which indicates that the Ti/Ta_2O_5−IrO_2 electrode has much larger real surface area than regular metal electrodes such as Pt due to the porous structure of the oxide coating as observed in the SEM images.

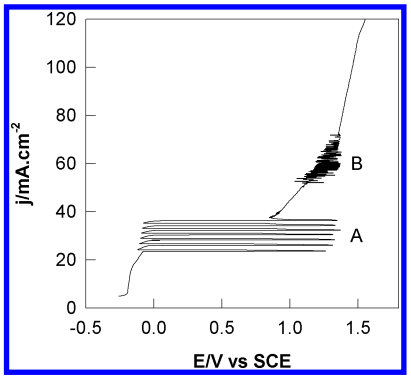

Figure 3. Linear galvanic voltammogram of 0.65 M Na_2S on the Ti/Ta_2O_5−IrO_2 electrode. Galvanic scan rate: 20 μA/s.

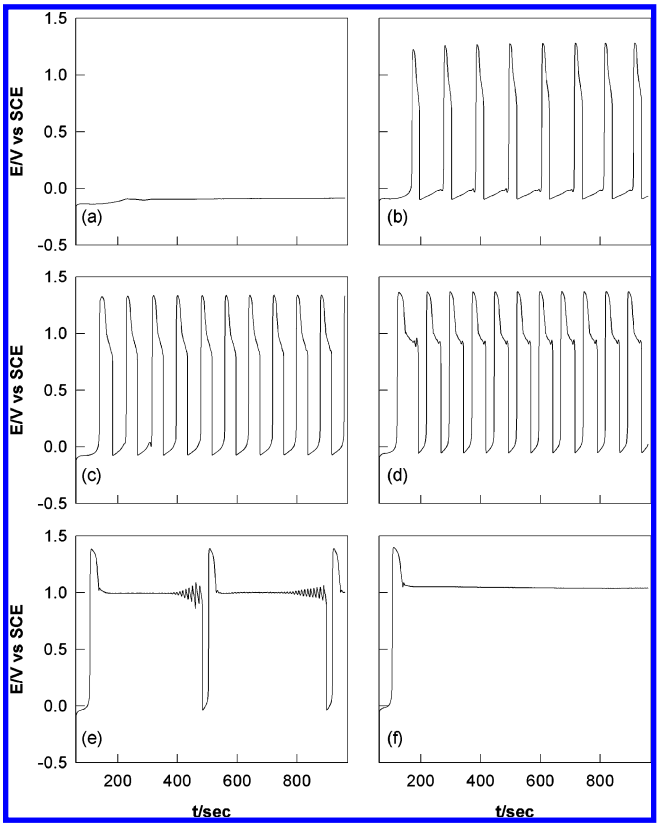

Figure 4. Chronopotentiometric curves of 0.65 M Na_2S: (a) 20 mA cm^{-2}; (b) 25 mA cm^{-2}; (c) 30 mA cm^{-2}; (d) 35 mA cm^{-2}; (e) 40 mA cm^{-2}; and (f) 45 mA cm^{-2}.

3.3. Galvanostatic Potential Oscillations during the Anodic Oxidation of Sulfide. Figure 3 shows a linear galvanic voltammetric curve recorded in the 0.65 M Na_2S solution from 5 mA to 150 mA at a current scan rate of 20 μA/s. Two different regions of potential oscillation are observed in the galvanic curve, named here as Oscillation A and Oscillation B, respectively. The amplitude of Oscillation A is significantly larger than that of Oscillation B. In contrast, the frequency of Oscillation A is much smaller than that of Oscillation B.

Figure 4 shows Oscillation A under galvanostatic conditions. In each galvanostatic experiment, the initial current density (j_1) was set at 0 mA/cm^2 for one minute. The current was then increased and held at j_2 for 15 min. At the low current density j_2 = 20 mA/cm^2 the potential increases slowly from −0.115 V, then stays at around −0.1 V, and no oscillations are observed.

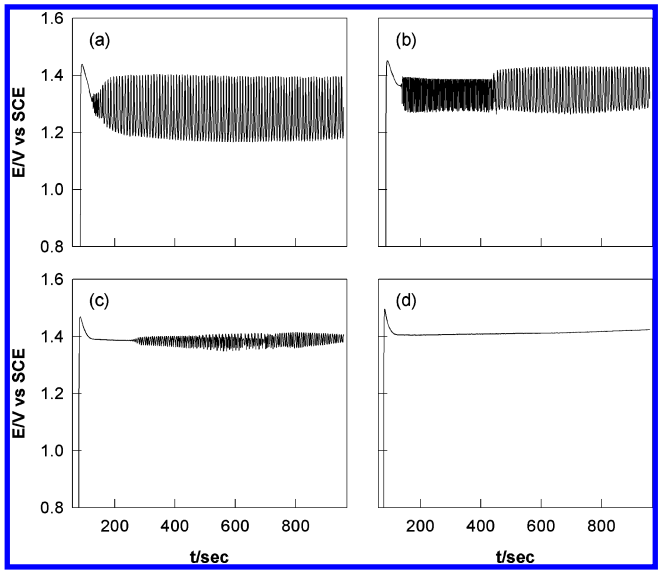

Figure 5. Chronopotentiometric curves of 0.65 M Na_2S: (a) 60 mA/cm^2; (b) 65 mA/cm^2; (c) 70 mA/cm^2; and (d) 75 mA/cm^2.

In contrast, periodic potential oscillations are observed when j_2 is increased to 25, 30, and 35 mA/cm^2. The amplitudes of these oscillations are very large, region between −0.1 V and +1.4 V/SCE, and remain almost the same size for these three different current densities. Initially, the potential increases slowly from −0.1 to 0.0 V. Once it reaches 0.0 V, the potential jumps to +1.4 V, then drops down to −0.1 V. The time to increase the potential from −0.1V to 0.0 V decreases when increasing j_2 from 25 to 35 mA/cm^2; thus, the frequency of the oscillations increases. On the other hand, there is a shoulder present at around 1.0 V when the potential drops from 1.4 to −0.1 V. This shoulder becomes more and more definitive with increasing current density. At 40 mA/cm^2, the shoulder becomes a platform and dominates the $E - t$ curve with some small oscillations and two large oscillations. When further increasing j_2 to 45 mA/cm^2, all oscillations disappear, and the electrode potential is slightly higher than +1.0 V. All these results show that the potential oscillations strongly depend on the applied current density.

Figure 5 presents four galvanostatic curves in the Oscillation B region. The potential oscillations with high frequency observed at 60 mA/cm^2 are between 1.15 and 1.4 V/SCE. Increasing the current density j_2, the upper boundary of the oscillations is still unchanged, but the bottom of the oscillations moves up. As a result, the amplitude of the oscillation becomes smaller and smaller. The oscillation vanishes at j_2 = 75 mA/cm^2, where the potential stays slightly above 1.4 V. As shown in Figure 2, there is no oscillation present in the CV curve, and we did not observe any potentiostatic current oscillations in our investigated potential range from −0.8 to 1.8 V, which is different from the behavior observed during the anodic oxidation of sulfide on the Pt electrode.[39] To understand the nature of the galvanostatic potential oscillations, we did further studies on sulfide oxidation using electrochemical impedance spectroscopy.

3.4. Electrochemical Impedance Study. Figure 6 presents six Nyquist plots at different electrode potentials, where Z_r and Z_i are the real and imaginary components of the impedance, respectively. The frequency was changed from 25 kHz to 25 mHz as indicated in the plots. The potential chosen in the EIS study was determined from the galvanostatic results. The behavior of the impedance plot at −0.05 V is totally different from the Nyquist plot recorded at −0.1 V; negative impedance appears at the potential −0.05 V. This is very consistent with

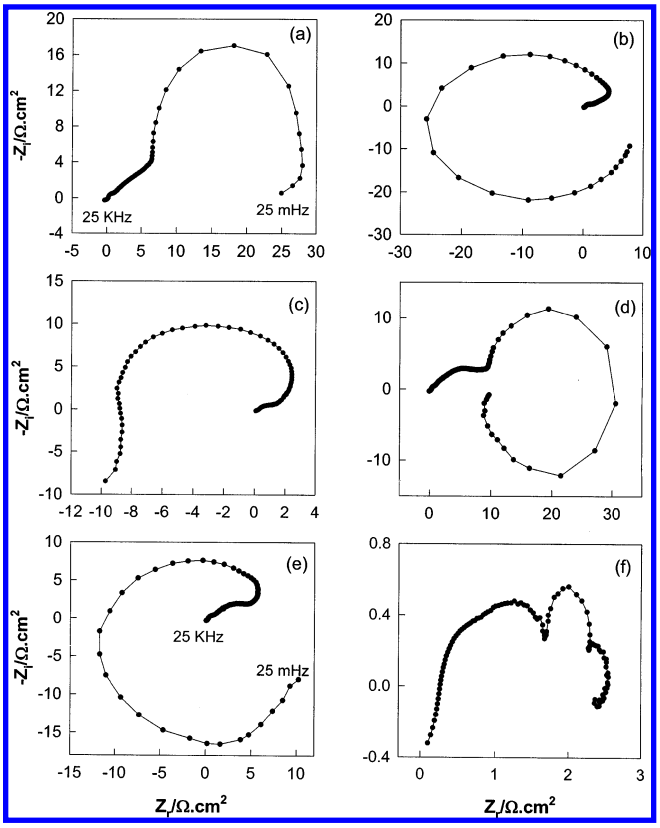

Figure 6. EIS complex plane plots of the Ti/Ta_2O_5−IrO_2 electrode in 0.65 M Na_2S with the electrode potential: (a) −0.1 V; (b) −0.05 V; (c) 0.5 V; (d) 1.0 V; (e) 1.2 V; and (f) 1.4 V.

the galvanostatic study: no potential oscillation is observed at 20 mA/cm^2 where the electrode potential is −0.1 V; and potential oscillations occur at 25 mA/cm^2 where the electrode potential is above −0.1 V. With increasing potential, negative faradic impedance is also observed at 0.5 and 1.2 V. Those two potentials lie in the range of the potential oscillations. All these results clearly show the presence of a hidden negative differential resistance (HNDR) (i.e., negative differential resistances in a region of intermediate frequencies and positive differential resistances in low frequencies). Thus, both Oscillation A and Oscillation B can be classified as HNDR oscillators with oxygen evolution involved, as shown later in the in situ images of the electrode surface. This conclusion can be further supported by the EIS results: the Nyquist plot at −0.05 V is similar to the plot at 1.2 V. At +1.0 and +1.4 V/SCE, only positive faradic impedance is seen. The oscillation vanishes at current density j_2 = 45 mA/cm^2 and 75 mA/cm^2, where the corresponding potential is around 1.0 and 1.4 V, respectively. The positive real impedance for 1.0 V is consistent with the galvanostatic results: a broad shoulder observed at the top part of the Oscillation A, and the potential range for Oscillation B is above 1.0 V. Moreover, three capacitive loops presented in the frequency-dependent impedance (Figure 6f) indicate a stable electrochemical system at 1.4 V with three chemical processes on different time scales.

3.5. Effect of Stirring and Purging on the Potential Oscillations. Figure 7 shows the effect of purging/stirring on the potential oscillations at 30 mA/cm^2. In Figure 7a, purging with ultrapure Ar starts at the bottom of the oscillation; while in Figure 7b, purging begins at the upper part of the oscillation. Curves 7a and 7b are almost identical, which indicates that the effect of purging is independent of the start point where the bubbling is applied during the potential oscillation. In Figure

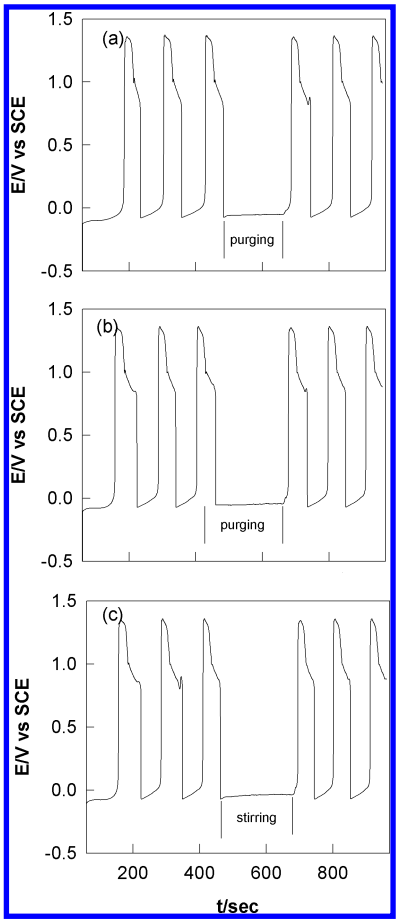

Figure 7. Stirring/purging effects on the chronpotentiometric curves of 0.65 M Na_2S at 30 mA/cm^2: (a) purging at bottom of the oscillation; (b) purging at top of the oscillation; (c) stirring at bottom of the oscillation.

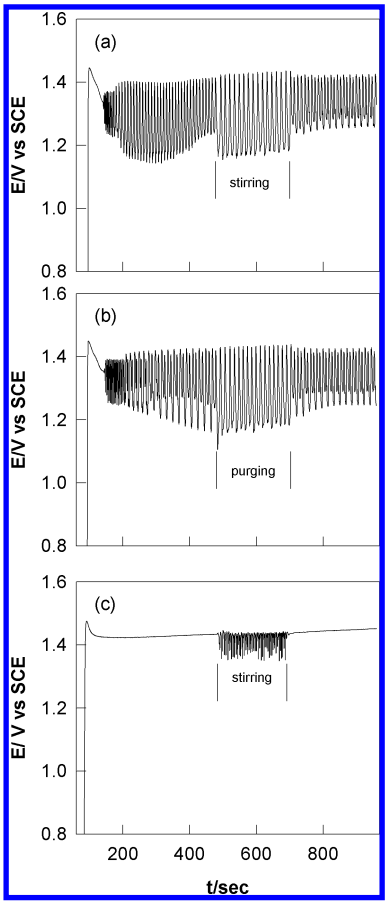

Figure 8. Stirring/purging effects on the chronopotentiometric curves of 0.65 M Na_2S at: (a) 60 mA/cm^2 (stirring); (b) 60 mA/cm^2 (purging); and (c) 85 mA/cm^2 (stirring).

7c, magnetic stirring was turned on at the bottom part of the oscillation. With either purging or stirring, the electrode potential stays at around −0.1 V and the oscillation disappears. This is consistent with the above impedance study, only positive impedance, rather than negative faradic impedance, was observed at the potential −0.1 V in the Nyquist plot. After the purging/stirring was turned off, the potential oscillations quickly recover to its initial behavior.

Figure 8 shows the effect of purging/stirring on the potential oscillations in the Oscillation B region. With either stirring or purging at j_2 = 60 mA/cm^2, the periodic potential oscillations still appear in the galvanostatic curve. The shape of the waveform is similar to that without stirring and purging. The frequency of the oscillations is only slightly different from that without stirring. The amplitude of the potential oscillation becomes slightly larger with the stirring/purging, between 1.15 and 1.4 V. Based on the results of our impedance study (negative impedance observed at 1.2 V/SCE) one can predict that the potential oscillations can occur in this potential range. As shown in Figure 8c, the electrode potential at 85 mA/cm^2 is higher than 1.4 V and no potential oscillation is present in the galvanostatic curve. However, when the stirring is turned on, the electrode potential is lowered and the potential oscillations appear. The oscillations vanish right away when the stirring is stopped. All of the above results are very consistent with our impedance study, and also indicate that mass transfer plays an important role in the potential oscillations during the electrooxidation of sulfide.

4. Oscillation Mechanisms

The mechanisms for the electrochemical oxidation of sulfide are complicated since sulfur has a number of different oxidation states such as −2, 0, +4, and +6. Anodic oxidation of sulfide can produce elemental sulfur, polysulfides, or sulfur oxyanions depending on the potential, pH, and temperature of the electrolyte. As described in section 3.2, the pH of the 0.65 M Na_2S electrolyte used in this study is close to the pH value of a 0.65 M NaOH solution, which indicates that HS^- ions are the predominant species. Some possible anodic reactions[37−38,40−41] are listed here:

$$HS^- + OH^- = S + H_2O + 2e^- \quad (1)$$

$$S^{2-} = S + 2e^- \quad (2)$$

$$2HS^- + 2OH^- = S_2^{2-} + 2H_2O + 2e^- \quad (3)$$

$$S_2^{2-} = 2S + 2e^- \quad (4)$$

$$HS^- + 9OH^- = SO_4^{2-} + 5H_2O + 8e^- \quad (5)$$

Figure 9 shows five in situ images of the electrode surface taken by a digital camera at 20 mA/cm^2 (image a) where no potential oscillation occurs, at 35 mA/cm^2 in the Oscillation A region (images c, d, and e), and at 65 mA/cm^2 (image f) where Oscillation B is located. Figure 9b indicates where the images c, d, and e were taken during the oscillation. Our galvanostatic study shows that the electrode potential is −0.1 V/SCE at 20 mA/cm^2. Under the potential −0.1 V, all the above listed anodic

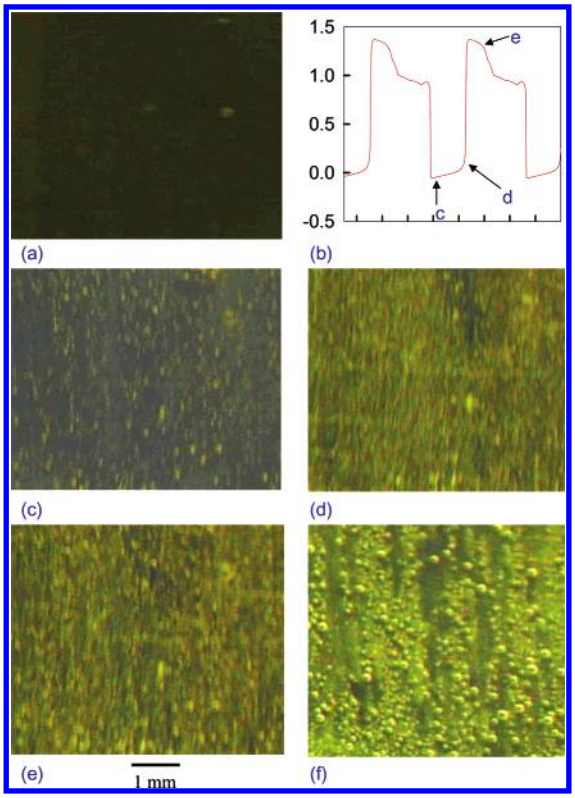

Figure 9. In situ images of the $Ti/Ta_2O_5-IrO_2$ electrode surface at 20 mA/cm^2 (a), at 35 mA/cm^2 (c, d, and e), and at 65 mA/cm^2 (f). Figure 9b indicates where the images c, d, and e were taken during the oscillation.

reactions can occur, except Reaction 5 as this takes place at much higher potential 1.1 V.[38] For instance, the electrode potentials for reactions 1 and 2 are −0.48 and −0.51 V/SCE, respectively.[41] Hydrosulfide can be oxidized to sulfur and/or polysulfides. Sulfide and polysulfides can also be oxidized to form sulfur. However, there is no sulfur build-up on the electrode surface as shown in image 9a. It has been reported that the sulfur layer can be dissolved by forming polysulfides,[42] i.e.,

$$S + HS^- + OH^- = S_2^{2-} + H_2O \quad (6)$$

$$S + S_2^{2-} = S_3^{2-} \quad (7)$$

Thus, one would not see sulfur build-up on the electrode surface, even if there were sulfur formation, if the dissolution of sulfur is faster than its formation. This is also supported by the results shown in Figure 8, the potential oscillations vanish and the electrode potential stays at around −0.1 V when the stirring/purging is turned on. The stirring/purging increases the mass transfer by moving HS^-, S^{2-}, and OH^- to the electrode surface and moving sulfur away from the electrode surface. There is no sulfur build-up on the electrode surface; thus, the potential oscillations vanish.

Figure 9b shows the potential oscillations at 35 mA/cm^2 in the Oscillation A region. As shown in Figure 9b, images c and d were taken at the bottom part of the oscillation, and image f was taken at the top portion of the oscillation. As seen in images c and d, when the electrode potential increases from −0.1 to 0.0 V, more and more sulfur deposits are formed on the electrode surface. The conductivity of the sulfur layer is very low and explains why negative impedance is observed in the impedance spectrum at −0.05 V. Once the electrode potential reaches approximately 0.0 V, it jumps to around +1.4 V, then drops slowly. When the potential is down to 0.9 V, it suddenly falls down to −0.1 V. As seen in image e, oxygen evolution is present in Oscillation A at the upper potential side, which stops at the lower potential side according to the experiment results (Figures 2a and 3). In other words, periodic oxygen evolution occurs in Oscillation A. In addition, Oscillation A appears above the limiting current (Figure 3) and the current for the backward scanning is larger than that for the forward scanning (Figure 2a) for a range of potentials, while the potential is reversed at 1 V where oxygen evolution occurs. Oscillation A stops by imposing a constant convection as no depletion could occur because of stirring or purging (Figure 7). Thus, the variation of the S^{2-}/HS^- surface concentration from the diffusion-limited depletion by oxidation and from the convection-induced replenishment by oxygen evolution might be the main reason for Oscillation A. The sulfur deposit/removal might also cooperate with the depletion/replenishment in Oscillation A, depletion accompanying sulfur deposition and replenishment accompanying sulfur removal. To test whether the sulfur deposits can be directly oxidized to sulfate or not, first we deposited sulfur on the electrode surface at 0.6 V for five minutes in a 0.65 M Na_2S solution, then transferred the electrode with sulfur deposits into a 0.65 M NaOH solution. After five-minute electrolysis at 1.4 V in the 0.65M NaOH, we still could see sulfur deposits on the electrode surface. Therefore, the removal of sulfur from the electrode surface is mainly through forming soluble polysulfides rather than through oxidation of sulfur into sulfate.

As seen in image 9f, there are sulfur deposits and gas bubbles on the electrode surface at 65 mA/cm^2, where Oscillation B is located. As seen in Figure 3, the potential range for Oscillation B is only a portion of that of Oscillation A. However, the rates for the electrode processes in Oscillation B are dramatically different from that in Oscillation A since Oscillation B appears at a much higher current range. Oscillation B is irregular, and has much smaller amplitudes and higher frequencies in comparison to Oscillation A. The surface concentration of S^{2-}/HS^- depletes much more rapidly (higher frequency), and the oxygen evolution immediately becomes predominant preventing the S^{2-}/HS^- surface concentration from completely restoring (smaller amplitudes). As a result, oxygen evolution behaves continuously and the surface sulfur deposit remains all the time as shown in Figure 9f, although their quantities may vary from time to time (irregular). An additional stirring is helpful to lower the potential by partial restoring the S^{2-}/HS^- surface concentration. The potential shifted more negatively due to the stirring as shown in Figure 8. All these results indicate that the Oscillation B is due to the synergic effect of sulfur formation/removal and constant oxygen evolution.

5. Summary

The electrooxidation of sulfide on a microstructured oxide electrode $Ti/Ta_2O_5-IrO_2$ has been investigated by a number of electrochemical methods such as cyclic voltammetry, differential capacity, galvanostatic measurements, and electrochemical impedance spectroscopy in this study. Sulfide and hydrosulfide can be oxidized to sulfur, polysulfides, and sulfate depending upon the electrode potential. The SEM analysis shows that the $Ti/Ta_2O_5-IrO_2$ electrode prepared in this study has a "cracked mud" structure with oxide particles sitting on the top. The particle size is around 100 nm. This oxide electrode has much larger surface area than planar metal electrodes such as Au and Pt. Two distinct ranges of galvanostatic potential oscillations, Oscillation A and Oscillation B, are observed during the

electrooxidation of sulfide on the oxide electrode. Oscillation A is in the range from 20 to 45 mA/cm^2, while Oscillation B is located in the region between 55 and 75 mA/cm^2. It is also found that mass transfer plays an important role in the potential oscillations. The variation of the S^{2-}/HS^- surface concentration from the diffusion-limited depletion by oxidation and from the convection-induced replenishment by periodic oxygen evolution might be the main reason for Oscillation A, while Oscillation B is due to the synergic effect of sulfur formation/removal and constant gas evolution. The EIS studies show that both Oscillation A and Oscillation B can be classified into a new type of HNDR oscillators with oxygen evolution involved. The oxide $Ta_2O_5-IrO_2$ is a promising electrocatalyst in the electrochemical treatment of sulfide solutions, and the influence of the oscillations on the lifetime of the $Ti/Ta_2O_5-IrO_2$ is being investigated by our group. In summary, we have demonstrated that the electrooxidation of sulfide on the oxide electrode $Ti/Ta_2O_5-IrO_2$ is an excellent system to examine the nature of the oscillations as one can directly observe the change of the electrode surface during the potential oscillations caused by sulfur formation/removal.

Acknowledgment. This work was supported by Lakehead University and a grant from the Natural Sciences and Engineering Research Council of Canada (NSERC).

References and Notes

(1) Hudson, J. L.; Tsotsis, T. T. *Chem. Eng. Sci*. **1994**, *49*, 1493.
(2) Wojtowicz, J. In *Modern Aspects of Electrochemistry*; Bockris, J., Conway, B., Eds.; Butterworths: London, 1973; Vol. 8, p 47.
(3) Costa, J. M.; Sagues, F.; Vilarrasa, M. *Phys. Rev*. **1991**, *A 43*, 7075.
(4) Degn, H. *J. Chem. Soc., Faraday Trans.* **1968**, *64*, 1348.
(5) Russel, P.; Newman, J. S. *J. Electrochem. Soc*. **1986**, *133*, 2093.
(6) Wojtowicz, J.; Marincic, N.; Conway, B. E. *J. Chem. Phys*. **1968**, *48*, 4333.
(7) Schell, M.; Albahadily, F. N.; Safar, J.; Xu, Y. *J. Phys. Chem*. **1989**, *93*, 4806.
(8) Hachkar, M.; Choy de Martinez, M.; Rakotondrainibe, A.; Beden, B.; Lamy, C. *J. Electroanal. Chem.* **1991**, *302*, 173.
(9) Schmidt, T. J.; Grgur, B. N.; Markovic, N. M.; Ross, P. N., Jr. *J. Electroanal. Chem.* **2001**, *500*, 36.
(10) Strasser, P.; Eiswirth, M.; Ertl, G. *J. Chem. Phys*. **1997**, *107*, 991.
(11) Strasser, P.; Lübke, M.; Raspel, F.; Eiswirth, M.; Ertl, G. *J. Chem. Phys*. **1997**, *107*, 979.
(12) Krausa, M.; Vielstich, W. *J. Electroanal. Chem*. **1995**, *399*, 7.
(13) Eiswirth, M.; Lübke, M.; Krischer, K.; Wolf, W.; Hudson, J. L.; Ertl, G. *Chem. Phys. Lett.* **1992**, *192*, 254.
(14) Wolf, W.; Lübke, M.; Koper, M. T. M.; Krischer, K.; Eiswirth, M.; Ertl, G. *J. Electroanal. Chem*. **1995**, *399*, 185.
(15) Mukouyama, Y.; Nakanishi, S.; Konishi, H.; Ikeshima, Y.; Nakato, Y. *J. Phys. Chem. B.* **2001**, *105*, 10905.
(16) Nakanishi, S.; Mukouyama, Y.; Karasumi, K.; Imanishi, A.; Furuya, N.; Nakato, Y. *J. Phys. Chem. B.* **2000**, *104*, 4181.
(17) Flatgen, G.; Wasle, S.; Lübke, M.; Eickes, C.; Radhakrishnan, G.; Doblhofer, K.; Ertl, G. *Electrochim. Acta* **1999**, *44*, 4499.
(18) Nakanishi, S.; Sakai, S.; Hatou, M.; Mukouyama, Y.; Nakato, Y. *J. Phys. Chem. B* **2002**, *106*, 2287.
(19) Li, Z. L.; Ren, B.; Xiao, X. M.; Zeng, Y.; Chu, X.; Tian, Z. Q. *J. Phys. Chem. A* **2002**, *106*, 6570.
(20) Radkov, E. V.; Ljutov, L. G. *J. Electroanal. Chem*. **1988**, *241*, 349.
(21) Li, Z. L.; Cai, J. L.; Zhou, S. M. *J. Chem. Soc., Faraday Trans*. **1997**, *19*, 3519.
(22) Xu, L. K.; Scantlebury, J. D. *J. Electrochem. Soc*., **2003**, *150*(6), B288.
(23) Gattrell, M.; MacDougall, B.; Henuset, Y. M.; Fournier, J. *J. Appl. Electrochem*. **2002**, *32*, 1303.
(24) Chen, G.; Chen, X.; Yue, P. *J. Phys. Chem. B* **2002**, *106*, 4364.
(25) Ferro, S.; De Battisti, A. *J. Phys. Chem. B* **2002**, *106*, 2249.
(26) Strasser, P.; Eiswirth, M.; Koper, M. T. M. *J. Electroanal. Chem*. **1999**, *478*, 50.
(27) Koper, M. T. M. *J. Electroanal. Chem*. **1996**, *409*, 175.
(28) Koper, M. T. M. *Electrochim. Acta* **1992**, *37*, 1771.
(29) Koper, M. T. M.; Sluyters, J. H. *J. Electroanal. Chem*. **1994**, *371*, 149.
(30) Strasser, P.; Lubke, M.; Eickes, C.; Eiswirth, M. *J. Electroanal. Chem*. **1999**, *462*, 19.
(31) Strasser, P.; Lubke, M.; Parmananda, P.; Eiswirth, M.; Ertl, G. *J. Phys. Chem*. **1998**, *102*, 3227.
(32) Strasser, P.; Eiswirth, M.; Koper, M. T. M. *J. Electroanal. Chem*. **1999**, *478*, 50.
(33) Behm, M.; Simonsson, D. *J. Appl. Electrochem.* **1997**, *27*, 507.
(34) Chen, A.; Lipkowski, J. *J. Phys. Chem. B* **1999**, *103*, 682.
(35) Chen, A.; Nigro, S. *J. Phys. Chem. B* **2003**, *107*, 13341.
(36) Comninellis, CH.; Vercesi, G. P. *J. Appl. Electrochem*. **1991**, *21*, 335.
(37) Szynkarczuk, J.; Komorowski, P. G.; Donini, J. C. *Electrochim Acta*, **1994**, *39*, 2285.
(38) Szynkarczuk, J.; Komorowski, P. G.; Donini, J. C. *Electrochim Acta*, **1995**, *40*, 487.
(39) Helms, H.; Schlomer, E.; Jansen, W. *Monatsh. Chem*. **1998**, *129*, 617.
(40) Ateya, B. G.; Al-Kharafi, F. M. *Electrochem. Commun.* **2002**, *4*, 231.
(41) Latimer, W. M. *The Oxidation States of the Elements and Their Potentials in Aqueous Solutions*, 2nd ed.; Prentice Hall, Inc.: Englewood Cliffs, N. J., 1952.
(42) Giggenbach, W. F. *Inorg. Chem.* **1974**, *13*, 1724.